Geophysical Research Letters

RESEARCH LETTER
10.1029/2019GL084686

Will the Surface Water and Ocean Topography (SWOT) Satellite Mission Observe Floods?

Renato Prata de Moraes Frasson[1], Guy J.-P. Schumann[2,3,4], Albert J. Kettner[4], G. Robert Brakenridge[4], and Witold F. Krajewski[5,6]

[1]Byrd Polar and Climate Research Center, Ohio State University, Columbus, OH, USA, [2]Remote Sensing Solutions, Inc., Barnstable, MA, USA, [3]School of Geographical Sciences, University of Bristol, Bristol, UK, [4]Dartmouth Flood Observatory, Institute of Arctic and Alpine Research, University of Colorado Boulder, Boulder, CO, USA, [5]Iowa Flood Center, University of Iowa, Iowa City, IA, USA, [6]Civil and Environmental Engineering Department, University of Iowa, Iowa City, IA, USA

Key Points:
- SWOT temporal and spatial observation capabilities and limitations are evaluated using recent floods in eastern Iowa and from Hurricane Harvey
- During its life cycle, SWOT may observe hundreds of flood events, including over data-scarce regions
- Dartmouth Flood Observatory data suggest that more destructive floods tend to last longer and are more likely to be observed by SWOT

Supporting Information:
- Supporting Information S1

Correspondence to:
R. P. d. M. Frasson,
frasson.1@osu.edu

Citation:
Frasson, R. P. d. M., Schumann, G. J.-P., Kettner, A. J., Brakenridge, G. R., & Krajewski, W. F. (2019). Will the Surface Water and Ocean Topography (SWOT) satellite mission observe floods? *Geophysical Research Letters*, *46*, 10,435–10,445. https://doi.org/10.1029/2019GL084686

Received 23 JUL 2019
Accepted 26 AUG 2019
Accepted article online 29 AUG 2019
Published online 7 SEP 2019

Abstract The Surface Water and Ocean Topography (SWOT) mission will measure water surface elevations and inundation extents of rivers of the world but with limited temporal sampling. By comparing flood location and duration of 4,664 past flood events recorded by the Dartmouth Flood Observatory to SWOT's orbit ephemeris, we estimate that SWOT would have seen 55% of these, with higher probabilities associated with more extreme events and with those that displaced more than 10,000 people. However, SWOT measurements will exhibit uneven temporal sampling and may require a combination of data obtained at different times to accurately characterize large events. This is illustrated using recent flooding in the United States, in eastern Iowa and in Houston and surrounding areas from Hurricane Harvey. SWOT data have significant potential to improve flood forecasting models by offering data needed to enhance flow routing modeling, provided that users can overcome the potential hurdles associated with its temporal and spatial sampling characteristics.

Plain Language Summary The Surface Water and Ocean Topography (SWOT) satellite mission will simultaneously measure water surface elevations and inundated areas for the Earth's land surface. Such information can be valuable for improving flood models and their calibration; however, SWOT temporal sampling will be limited, with most locations in the world being seen once every 7 to 10 days, which may cause it to miss floods. Using a record of global flood information, including duration and location, compiled by the Dartmouth Flood Observatory and the expected satellite orbit, we estimated that, if already operational, SWOT would have collected at least one measurement over 55% of these events. We illustrate SWOT data coverage using flood inundation maps generated for flooding in eastern Iowa (2008) and in Houston and surrounding areas, Texas, caused by Hurricane Harvey (2017). Due to the novelty of this kind of hydrological information, particularly in the way SWOT samples rivers in time and space, early engagement of potential users may be instrumental to maximize the utility of this open source of worldwide observations of rivers, lakes, and inundated land.

1. Introduction

Floods are linked to many fatalities each year and to billions of dollars in property damage in the United States alone (Pielke & Downton, 2000; Wing et al., 2018). Quinn et al. (2019) estimated a 1% chance of damages exceeding $78 billion due to fluvial floods in the United States in any given year. With recovery periods becoming shorter in some regions due to increased flood frequencies (e.g., Mallakpour & Villarini, 2015), it is valuable to have quick access to data on current and past watershed conditions. Remote sensing has the potential to complement the existing network of in situ instruments: by filling in the gaps in sparse stream gauge networks (Alsdorf et al., 2007; Pavelsky et al., 2014; Tarpanelli et al., 2019), by offering worldwide or near-worldwide coverage (Biancamaria et al., 2016), and by mitigating data sharing barriers for international river basins (e.g., Gleason & Hamdan, 2015; Hossain et al., 2014; Sneddon & Fox, 2006, 2012; Wolf et al., 1999).

The upcoming Surface Water and Ocean Topography (SWOT) internationally supported (United States, France, Canada, and United Kingdom) satellite mission will continuously measure water surface elevation and inundation areas of rivers wider than 100 m and lakes larger than 62,500 m^2, with nearly global coverage

(e.g., Biancamaria et al., 2016; Durand et al., 2010; Rodríguez, 2015). However, SWOT data will have limited temporal sampling, which may interfere with its ability to observe flood events.

Biancamaria et al. (2016) estimate typical SWOT revisit periods to be one to two observations every 20.86 days for locations between 20°S and 20°N and two or more at higher latitudes. Our goal here is to assess the impact of SWOT's temporal resolution on its ability to detect floods. To fulfill this goal, we use a flood database compiled by G. R. Brakenridge and associates at the Dartmouth Flood Observatory (hereafter DFO; accessible through http://floodobservatory.colorado.edu/), which provides records of flood duration, cause, location, start and end dates, and socioeconomic impacts of floods, globally, since 1985 (Adhikari et al., 2010; Kundzewicz et al., 2013).

We begin with a short description of the future SWOT measurements (section 2), after which we present the method used to identify which flood events would have been observed if the satellite was operational. We thereby estimate either the probability of detection of events or the guaranteed number of measurements per event (section 3). We analyze the probability of detections and their geographical distribution in section 4 and provide overall conclusions in section 5.

2. SWOT Observations

SWOT will orbit Earth at an altitude of 890.5 km and inclination of 77.6°, with an exact orbit repeat period of 20.86 days (Biancamaria et al., 2016). The 21-day cycle is divided into 585 passes: the path that the satellite follows as it travels from the most southern point to its most northern point (ascending pass) or from north to south (descending pass). SWOT's main instrument is a Ka-band radar interferometer, which uses two antennas separated by 10 m to illuminate two 50-km swaths over the Earth surface. A graphical representation of the swaths is shown in Figure S1a in the supporting information. The swaths, located at both sides of the spacecraft's ground track, are separated by a 20-km nadir gap: an area immediately below the satellite which is not surveyed during the overpass.

SWOT's basic measurements are the returned microwave power and range to the ground target and the difference in phase in the return signal received by both antennas. At near-nadir incidence angles, water is more reflective to Ka-band than land surfaces; therefore, the magnitude of the returned power will be used to distinguish water from land (Biancamaria et al., 2016; Fjørtoft et al., 2014). The phase difference between the two antennas, the altitude of the spacecraft, and a reference digital elevation model of the surrounding terrain are used to simultaneously compute the geographical coordinates and the elevation of the water targets in a process called geolocation, which resembles triangulation (Fjørtoft et al., 2014).

The geolocated targets lie on an irregular grid resembling a cloud of points, or pixel cloud (Domeneghetti et al., 2018; Frasson et al., 2017). The pixel size in the grid depends on its distance to the SWOT ground track, with its cross-track resolution varying from 60 m at the near range to 10 m at far range and its along-track resolution fixed at 6 m as illustrated in Figure S1a. Each pixel carries information on how much of its area is believed to be inundated, the water surface elevation, and target brightness and interferometric coherence, from which data quality can be assessed.

The standard deviation of pixel height errors are expected to be on the order of meters (Domeneghetti et al., 2018). However, spatial aggregation can mitigate water surface elevation noise, also allowing the computation of water surface slopes, resulting in height and slope errors on the order of 10 cm and 1.7 cm/km or less for a 100-m-wide river averaged over a 10-km-long reach (Biancamaria et al., 2016; Esteban-Fernandez, 2013; Frasson et al., 2017; Rodríguez, 2015). Additionally, from the inundation area of pixels contained within a reach, one can estimate average reach widths, which after several cycles can be stacked according to reach averaged heights to produce height-width curves.

An interesting feature of SWOT data will be the ability to construct continuous water surface profiles of rivers. Depending on river orientation and position with respect to the swath, profiles can be longer than 150 km as illustrated for the Sacramento River, which runs mostly in the north-south direction (Frasson et al., 2017), or 120 km with a 20-km nadir gap for the Po River, which runs west to east, as shown by Frasson et al. (2017) and Domeneghetti et al. (2018). When aggregated into points located every 200 m over river centerlines, called river nodes, the resulting profiles can be used to detect abrupt changes in the water surface elevation, indicative of hydraulic structures (Frasson et al., 2017), or be assimilated into one-dimensional

hydraulic models to estimate discharge (e.g., Brisset et al., 2018; Oubanas et al., 2018). River nodes can be further aggregated into reaches, thus allowing for estimation of water surface slopes. The retrieval of water surface elevations and calculation of slopes based on noisy elevation measurements is demonstrated by Altenau et al. (2017), Altenau et al. (2019), and Tuozzolo et al. (2019), who estimate reach-averaged slopes using water surface elevation measurements obtained by an airplane-mounted Ka-band radar interferometer (AirSWOT), for the Tanana and Willamette Rivers, USA.

Various studies describe the use of remote sensing to map floods and assess flood risks (e.g., Adhikari et al., 2010; Andreadis et al., 2017; Brakenridge, 2018; Van Dijk et al., 2016) and data collected by a constellation of satellites has been used to calibrate and validate hydraulic models (e.g., Bonnema & Hossain, 2017; Domeneghetti et al., 2014). However, unlike traditional nadir altimeters, SWOT will measure water surface elevations and inundation areas simultaneously, which is unprecedented from a single sensor. Additionally, due to its operating frequency, SWOT can penetrate clouds, obtaining inundation extent measurements in situations where optical sensors cannot observe, thus offering a new opportunity to track river and floodplain dynamics (Allen et al., 2018; Bates et al., 2014).

3. Materials and Methods

DFO provides a database containing information on flood duration, cause, location (an indicative polygonal outline of "flood-affected area"), reported fatalities, and damage that spans from 1985 to the present (Adhikari et al., 2010). We accessed the DFO repository on 31 August 2018, which at the time included information on 4,664 flood events. Relevant predicted satellite passes for each flood event catalogued by DFO were identified by comparing the distance between the flood polygon centroid and the ground track corresponding to each of the hypothetical 585 SWOT passes.

A flood event is considered "detected" by a particular SWOT pass if the distance between the flood centroid and the ground track is larger than or equal to 10 km (inner swath edge) and smaller than or equal to 60 km (outer swath edge), with graphical representation included in Figure S1b. We estimate the average time between SWOT visits by dividing the repeat cycle (20.86 days) by the number of swaths that intersected the centroid of each of the flood events. Finally, we compute the ratio between the flood duration and the time between SWOT observations, which, if equal to or less than 1, can be interpreted as the probability that the flood would have been observed by SWOT. Ratios larger than 1 indicate a probability of detection equal to 1; the value of the ratio in this case indicates the guaranteed number of observations of the flood event.

We utilize the ratio between flood duration and average time between observations to assess the number of flood events that would have been observed by SWOT. We consider three levels of observations: (1) likely observed, (2) guaranteed to be observed at least once during the flood, and (3) observed twice or more throughout the duration of the event. We built a histogram of probability of observations using classes with width equal to 0.1. The number of observed events per probability class is approximated by multiplying the number of events on each class by its central probability, which when added over all probability classes allows an estimate of the number of DFO-recorded events that would have been likely observed. The number of events in the second and third levels of observation were determined by counting the number of flood events with a ratio between duration and time between observations equal to or larger than 1 and in excess of 2, respectively.

4. Results and Discussion

Figure 1 summarizes the probabilities of detection per flood event. Figure 1a shows the histogram of the ratio between flood duration and average time between SWOT observations, whereas Figure 1b shows the empirical cumulative distribution function associated with this ratio. The ratio between flood duration and mean time between SWOT observations is converted into probability by assigning a probability of 1 to any ratio greater than 1. We thereby estimate that 55% of the DFO floods would have been observed if SWOT was operational or 2,565 events out of the 4,664 database entries.

The 4,664 database entries were recorded between 1985 and *31* August 2018, a period much longer than the expected three-year duration (Rodríguez, 2015) of the SWOT mission. However, exploring the entire

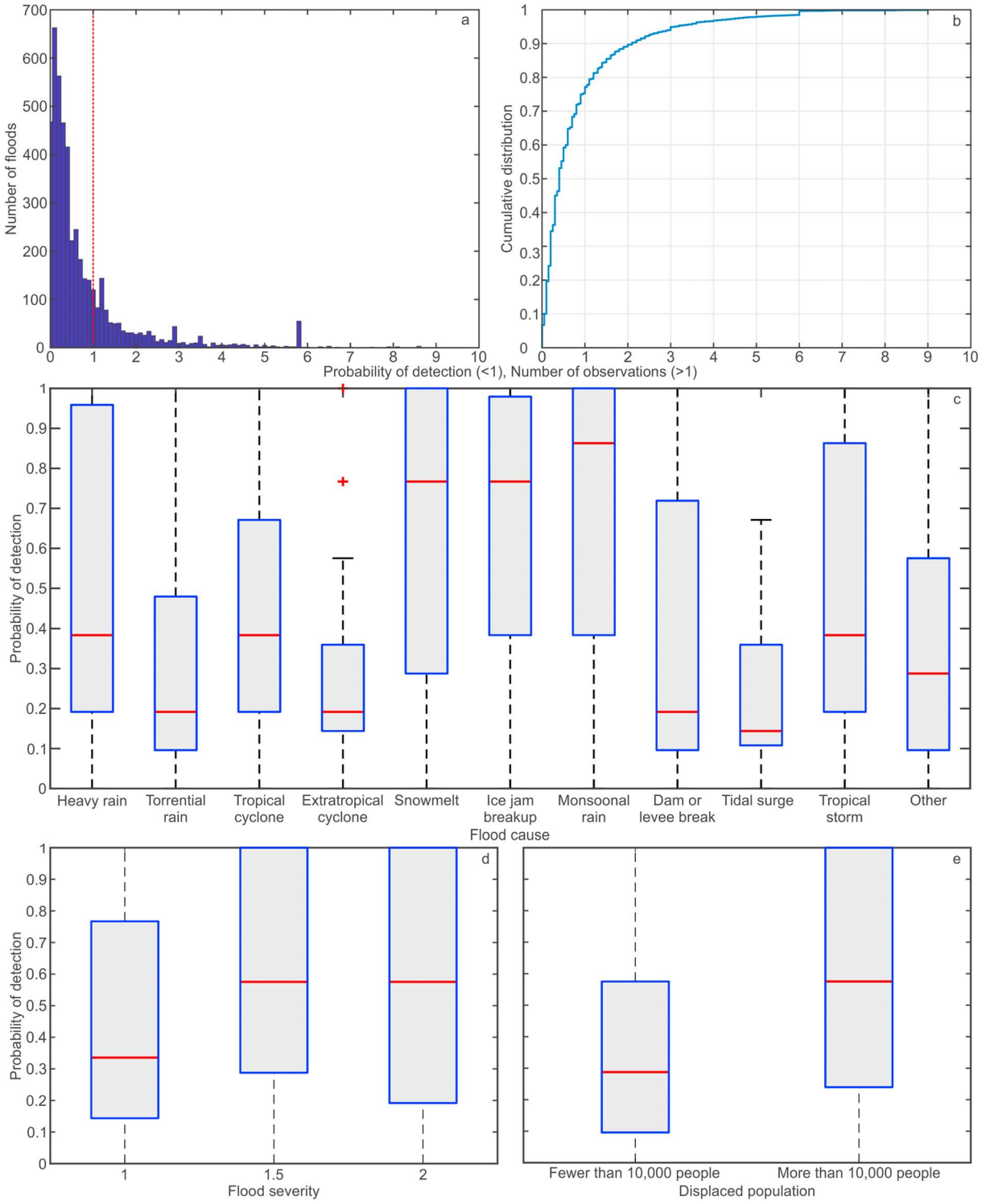

Figure 1. (a) The histogram of the ratio between the flood duration and the mean time between observations. Ratios less than or equal to 1 can be interpreted as the probability of detection, whereas ratios greater than 1 represent the number of times a flood would have been observed. (b) The corresponding cumulative distribution. (c) Box plots of the probability of detection for each reported flood cause. (d) Box plots of the probability of detection for three severity classes: 1—large flood events with return period of 10 to 20 years, 1.5—very large events with return period between 20 and 100 years, and 2—extreme events with estimated recurrence interval greater than 100 years. (e) Probability of detection grouped by the size of the displaced population. The number of events per cause, severity, and displaced population classes can be found in Tables S1–S3 in the supporting information, respectively.

duration of the DFO database provides a better sample of flood durations and a more robust estimate of the fraction of floods that are likely to be observed by SWOT which can then be applied to groups of three consecutive years. Regarding the number of catalogued floods per year, 1987 had the least number of recorded floods (45), and 2003 showed the largest number of flood events (297). Considering a fraction of observed floods of 55% applied to three successive years shows that SWOT would observe between 88 (55% of the floods recorded in 1985, 1986, and 1987) and 413 events (2002–2004), with a typical value (the median number of observed events per three-year period) of 198 events.

Figure 1c shows how the probability of detection varies for different flood causes. Notably, three types of floods have higher probability of detection: those caused by snowmelt, ice jam breakup, and those caused by monsoons. While floods caused by snowmelt and ice jam breakup happen characteristically at higher latitudes, where temporal sampling is denser, floods caused by monsoons have longer durations, which balances the sparser time sampling typical of tropical regions. Additionally, Figure 1c shows four categories with particularly low probability of detection: floods following torrential rains, dam or levee breaks, extratropical cyclones, and tidal surges, all of which tend to show positively skewed probability of detection distributions.

Furthermore, the DFO classifies its records into three flood severity categories: 1—large flood events with significant damage to structures or agriculture and/or estimated recurrence interval between 10 and 20 years, 1.5—very large events with recurrence intervals greater than 20 years but less than 100 years, and 2—extreme events with an estimated recurrence interval greater than 100 years. Grouping probabilities according to flood severity shows that more severe events (class 1.5 and 2) have higher probability of being observed at least once (Figure 1d). The association between severity and probability of detection is even more visible when probabilities are grouped by the magnitude of the displaced population. Figure 1e shows that floods that displace 10,000 or more people have a significantly higher probability of detection than those that displaced less than 10,000.

The latitude of a flood controls the number of revisits per cycle and thus the mean time between SWOT observations. However, when we mapped the probability of detection of the DFO-recorded floods (Figure 2a), we did not observe the probability of detection systematically increasing with higher latitudes (Figure 2c). The lack of this expected correlation between latitude and probability is because flooding that occurs in the tropical regions commonly lasts longer than floods at higher latitudes, thereby balancing the decreasing SWOT sampling frequency. Figure 2b shows the guaranteed number of observations per flood event and is a good indication of the potential SWOT may offer to flood modelers, first responders, and water managers for typical flood events.

Figure 2 provides conservative estimates of the probability of detection and the number of observations per event for three reasons: (a) if the ratio between flood duration and mean time between observations is one, then this flood could potentially be observed twice, depending on the start date of the flood; (b) observations of river height immediately before a flood may be of importance for flood forecasting, but we use strictly the flood duration reported by DFO; and (c) when selecting the passes that observed a flood event, we considered only those that intersected with the centroid of a flood. However, for riverine floods, observations upstream of a region of interest may carry substantial information about future conditions at a downstream location. For example, upstream discharge is a strong predictor of downstream discharge once travel time is accounted for (Biancamaria et al., 2011) and in the absence of significant contributions from tributaries.

While associating waterbodies with flood events could potentially allow us to extend the window of significance beyond flood duration, as well as extract information on river width and floodplain extent from global databases (e.g., Allen & Pavelsky, 2018; Nardi et al., 2019 respectively), water surface slope, meander wavelength, sinuosity, and discharge from Frasson et al. (2019), flood wave travel time from Allen et al. (2018), and others, such association is difficult to be automated without extensive manual intervention. Therefore, we present two case studies where we show the timing of SWOT passes with respect to flood hydrographs and display relevant SWOT swaths over the study areas, illustrating how spatial coverage may be during real flood events. The two case studies are the 2008 flood of Eastern Iowa, USA (Chen et al., 2017; Smith et al., 2013), and the 2017 flood of the Houston metropolitan area, USA, caused by Hurricane Harvey (Risser & Wehner, 2017; Zhang et al., 2018).

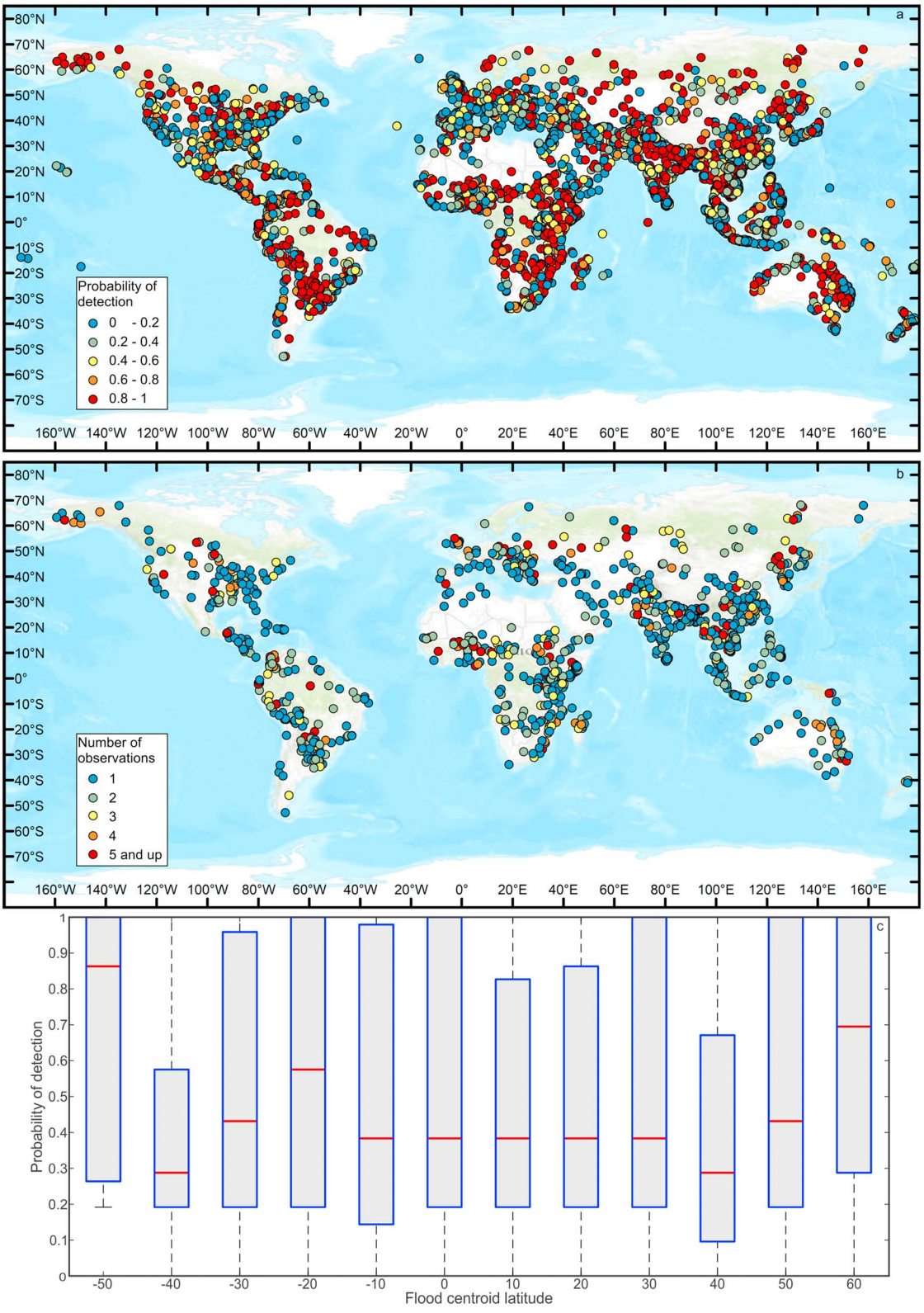

Figure 2. (a) The probability of detection of all 4,664 floods in the DFO database from 1985 to 31 August 2018. (b) Floods that were certain to be observed if SWOT was already operational, color coded to represent how many times the flood would have been observed by the satellite. (c) Box plots of the probability of detection grouped by the latitude of the flood.

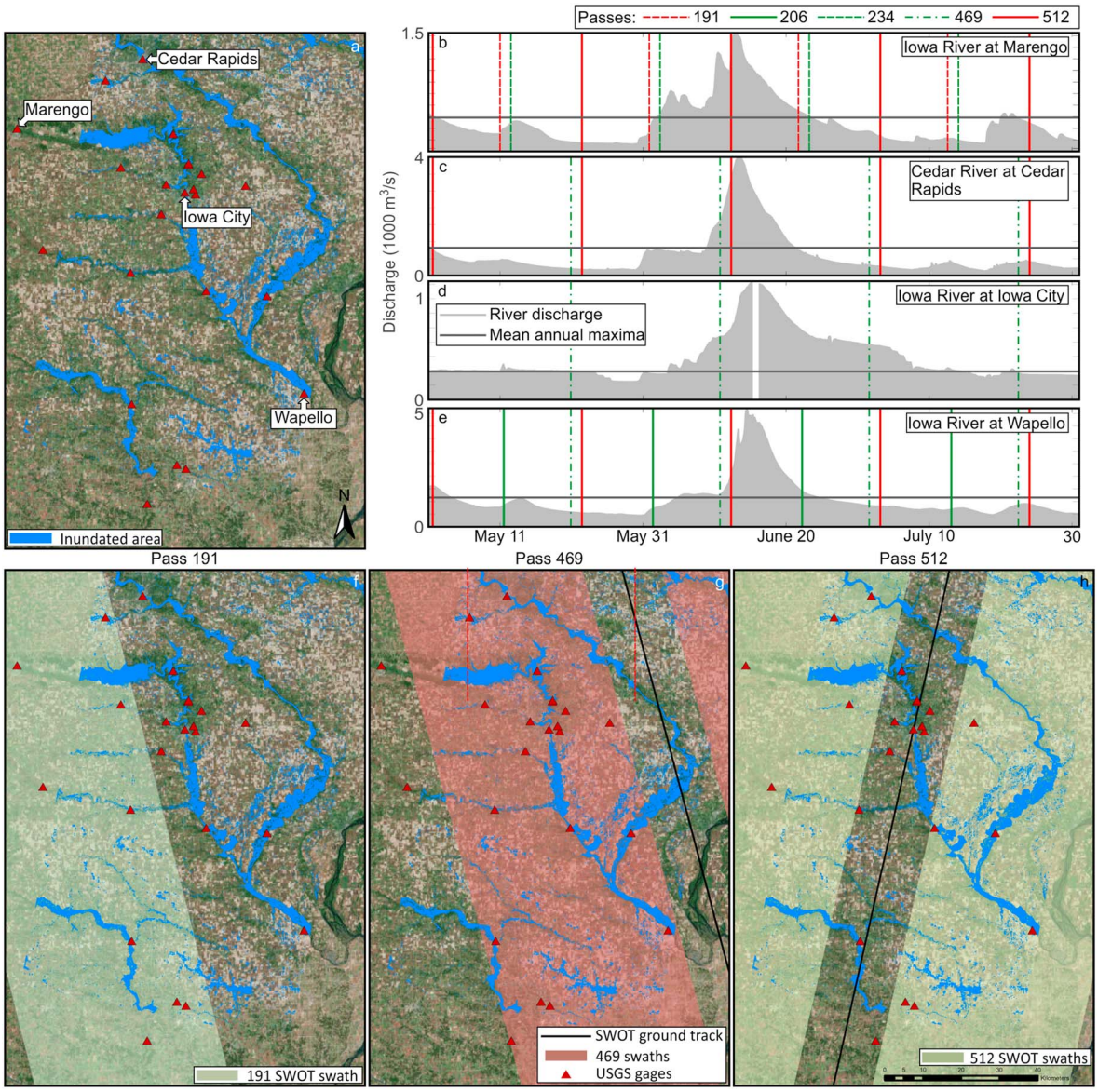

Figure 3. (a) The flood extent (in blue) recorded in eastern Iowa in the summer of 2008 and locations of USGS streamgage (red triangles) in the area. The flood propagated from northwest to southeast. (b–e) The flood hydrographs in Marengo, Cedar Rapids, Iowa City, and Wapello, respectively, where the vertical lines show SWOT overpass times if SWOT had been operational in 2008. (f–h) The areas observed by the SWOT swaths during the relevant passes superimposed on the maximum flood extent (in blue).

Figure 3a illustrates the inundation extent (in blue) of the Cedar and Iowa Rivers derived from high-resolution imagery obtained by the SPOT satellite (Kollasch, 2009) acquired in the days following the peak flow (17 July 2008) and also the location of the United States Geological Survey (USGS) gages (red triangles). Four of the available USGS gages provide flood hydrographs (Figures 3b–3e) for the event. To illustrate the SWOT spatial-temporal sampling, we identify three relevant passes while assuming an arbitrary start date for the SWOT cycles on 1 January 2008. Observation times are selected over each of the streamgages, shown as vertical lines superimposed on the hydrographs (Figures 3b–3e). Locations such as the Iowa River gage at Marengo would have been sampled four to five times during the period of interest (when the discharge exceeded annual peak flow). The Cedar River in Cedar Rapids and the Iowa River at Iowa City would have been observed by SWOT at least twice (Figures 3c and 3d, respectively), while the Iowa River at Wapello would have been sampled three times (Figure 3e).

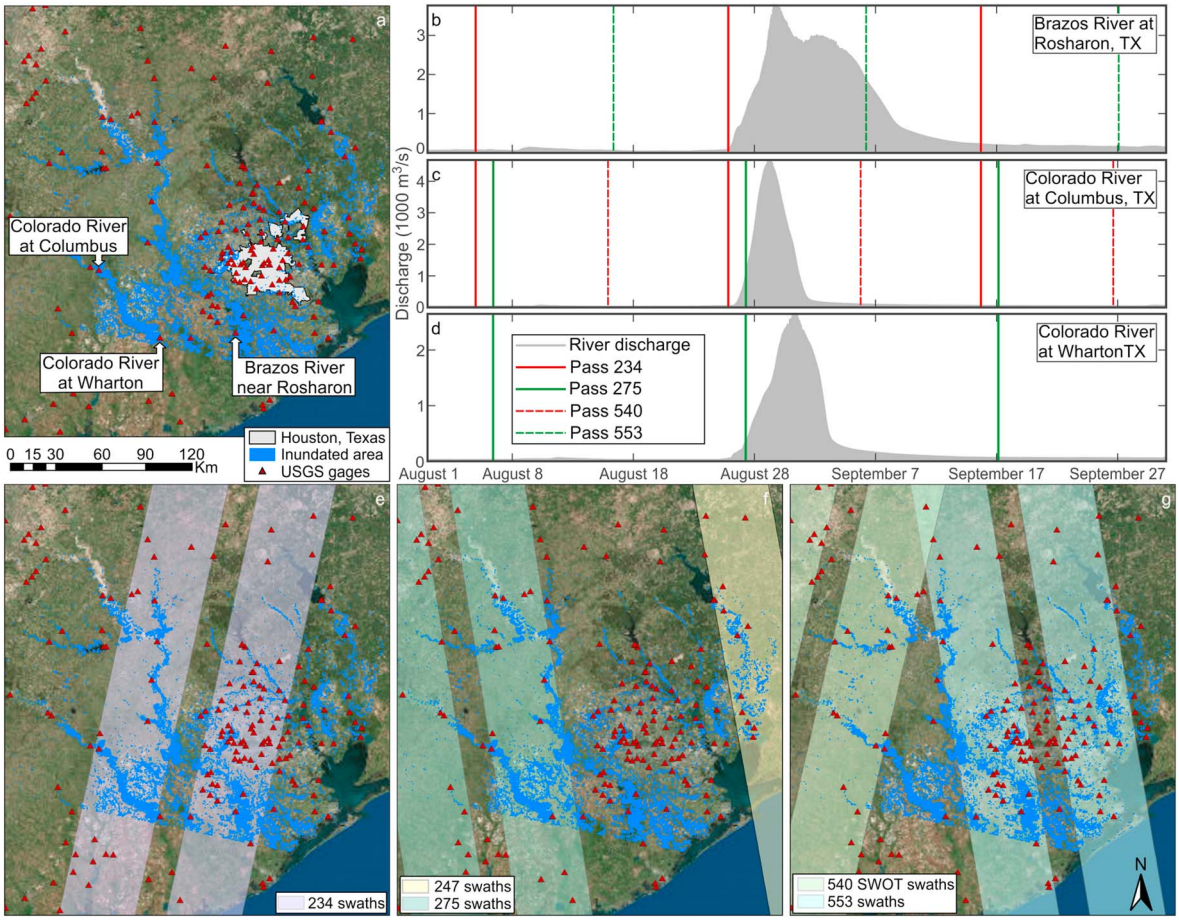

Figure 4. The flooding of Houston and surroundings caused by Hurricane Harvey, 2017. (a) The inundation area (in blue) detected by the Sentinel-1 satellite on 30 August 2017 after exclusion of permanent water bodies, with the Houston metropolitan area shown in gray, and the position of the USGS streamgages (red triangles). (b–d) The hydrographs of three streamgages with the timing of SWOT passes indicated by the vertical lines. (e–g) The five relevant swaths, over which SWOT would have collected water surface observations, if operational during the Hurricane Harvey superimposed on the inundation map produced for 30 August 2017.

Figures 3f–3h show the ground track and the swaths of the three relevant passes (191, 469, 512) in chronological order, superimposed on the inundation maps. Pass 191 does not intersect the centroid of this flood; however, it provides information on the upstream sections of the rivers, which offer information on the incoming flood wave. Additionally, pass 469 would have shown a long, continuous profile of the Iowa River and sections of the Cedar River, which provides useful information for the calibration and validation of local flood hydraulic modeling. Despite the swath gap of pass 512 falling over most of the Iowa River shown in the study area, leaving the area unobserved, this pass would produce a long profile of elevations over the Cedar River.

At mean annual flow, the section of the Iowa River depicted in Figure 3 has widths between 50 and 100 m, that is, below the required observation threshold, but above the detection limit of 50 m. This means that at or below mean annual flow, SWOT measurement uncertainty would likely be higher than the 10-cm water height accuracy for reaches and 1.7 cm/km for reach slopes (Desai, 2018; Rodríguez, 2015). Nevertheless, smoothing techniques presented by Frasson et al. (2017) and applied to AirSWOT data by Tuozzolo et al. (2019) can improve measurement accuracy, especially when their application can be done with supervision.

SWOT measurements over urban areas can have higher uncertainty than those listed by Desai (2018) and Rodríguez (2015). Structures neighboring rivers may introduce four sources of error: beam blockage, a situation when the river would be obscured by surrounding terrain or buildings; terrain layover, when returns from water and surrounding terrain reach the satellite simultaneously leading to positive biases

(Domeneghetti et al., 2018; Fjørtoft et al., 2014; Frasson et al., 2017); multipath propagation caused by reflection of radar signals on the sides of buildings before reaching water surfaces leading to increased random errors as well as biases; and bright roofs, when structures may appear bright and therefore may be erroneously classified as water. Moreover, although SWOT's resolution of 60 m by 6 m at the near range and 10 m by 6 m at the far range (Figure S1) will be too coarse to resolve flows around densely built environments, it may be useful for delineation of inundation extents. While such issues can be manually resolved at local scales, they will incur in higher uncertainty for both water surface elevations and inundation extents at regional to larger scales. Furthermore, flashfloods on urban settings or otherwise have durations much shorter than the typical SWOT revisit time exemplified in Figures 3 and 4, rendering such types of events incompatible with SWOT temporal sampling.

Figure 4 compares the SWOT swath with the inundation caused by Hurricane Harvey. Figures 4a and 4e–4g show the inundated area based on processing of Sentinel-1 Synthetic Aperture Radar observations collected on 30 August 2017 (Brakenridge & Kettner, 2017) with the Houston metropolitan area highlighted in gray in Figure 4a. Given the lower latitude of Houston as opposed to eastern Iowa, SWOT temporal sampling is sparser. Due to the large flood extent, a mosaic built with several passes is necessary to cover the whole affected area. Some areas may be observed as waters rise (e.g., Figures 4c and 4d), while others may be monitored as the flood declines: both can provide insight into different aspects of disaster response and flood management, that is, how quickly or widespread a flood event might be, how quickly waters may recede, knowledge of which can improve resource allocation and better target relief operations. If SWOT information reaches the end users quickly, it can be valuable for disaster management (Allen et al., 2018). However, even if flood data are only available sometime after the fact, they can still be of value for, namely, diagnostic and improvement of forecast inundation models, identification of poorly modeled areas, and possibly contribute to refining floodplain DEMs (Shastry & Durand, 2019). Furthermore, repeated SWOT passes over an area will allow the creation of relationships between water surface elevation and inundation extent, which can be used in conjunction with inundation maps generated from other platforms, such as Sentinel 1 to provide denser time series.

5. Conclusion

The SWOT mission will augment our ability to detect and size floods by simultaneously measuring water surface elevation and inundation extents over 120-km-wide swaths with a 20-km nadir gap, a novel capability compared to other remote sensing platforms such as the SPOT and Sentinel 1. SWOT will measure water surface elevation and slopes as well as inundation extents of rivers wider than 100 m and possibly as narrow as 50 m and measure inundation extents and elevations of lakes as small as 62,500 m^2 day and night and through clouds. Even if only available after the end of a flood event, SWOT-derived water elevation profiles of rivers can provide valuable information for the calibration and validation of hydraulic, hydrologic, and geomorphic floodplain extent models.

In some cases, floods cover very extensive geographic areas with persistence measured in weeks (e.g., Brahmaputra River flooding, reaching 5-km widths, at least, each year; Great Mississippi and Missouri Rivers Flood of 1993). In the latter example, levee failures caused dramatic changes in river elevations as the flood wave traversed downstream, and flood water reached different maximum levels on different sides of the trunk streams due to tributary discharge and backwater effects (Brakenridge et al., 1994). Flood waves may require several days to traverse downstream; it is also likely that SWOT will, therefore, directly measure such waves along flooding rivers and provide useful information for comparison to hydraulic modeling (Brakenridge et al., 1998).

Long-duration floods, which may be the most destructive and most severely affect local populations, are not only more likely to be observed, but also will likely be observed more than once. Such observations can, in turn, provide insight into how riverine floods propagate through the river network, spread across floodplains, are affected by levees and levee failures, and how they dissipate. However, SWOT data are irregular in spatial-temporal sampling. Locations with latitudes between 20°S and 20°N will be observed once or twice every 20.86-day cycle, while higher latitudes will be sampled typically 2 or more times per cycle. Sites that are observed by multiple passes will have uneven temporal sampling, which is one characteristic that must be accommodated by the end users. Because of the novelty of this kind of hydrological information, early

engagement of potential users, that is, through workshops promoted by the SWOT early adopters community coordinated by the SWOT applications working group (https://swot.jpl.nasa.gov/applications.htm) as well as the use of the soon to be released example data products may be instrumental to maximize the utility of this open source of worldwide observations of rivers, lakes, and inundated land.

Acknowledgments
R.P.d.M. Frasson and G.J.-P. Schumann would like to acknowledge the support received through the NASA SWOT Algorithm Definition Team contract to the Ohio State University and Remote Sensing Solutions Inc., respectively. Data used in this study are available from the DFO institutional repository at http://floodobservatory.colorado.edu/Archives. The inundation extents shown in Figure 3 are available from Kollasch (2009) and the inundation extents shown in Figure 4 are available from Brakenridge and Kettner (2017). The authors would like to thank the Editor and two anonymous reviewers for their constructive and insightful comments and suggestions.

References

Adhikari, P., Hong, Y., Douglas, K. R., Kirschbaum, D. B., Gourley, J., Adler, R., & Robert Brakenridge, G. (2010). A digitized global flood inventory (1998–2008): Compilation and preliminary results. *Natural Hazards*, *55*, 405–422. https://doi.org/10.1007/s11069-010-9537-2

Allen, G. H., David, C. H., Andreadis, K. M., Hossain, F., & Famiglietti, J. S. (2018). Global estimates of river flow wave travel times and implications for low-latency satellite data. *Geophysical Research Letters*, *45*(15), 7551–7560. https://doi.org/10.1029/2018GL077914

Allen, G. H., & Pavelsky, T. M. (2018). Global extent of rivers and streams. *Science*, *361*(6402), 585–588. https://doi.org/10.1126/science.aat0636

Alsdorf, D. E., Rodríguez, E., & Lettenmaier, D. P. (2007). Measuring surface water from space. *Reviews of Geophysics*, *45*, RG2002. https://doi.org/10.1029/2006RG000197

Altenau, E. H., Pavelsky, T. M., Moller, D., Lion, C., Pitcher, L. H., Allen, G. H., et al. (2017). AirSWOT measurements of river water surface elevation and slope: Tanana River, AK. *Geophysical Research Letters*, *44*, 181–189. https://doi.org/10.1002/2016gl071577

Altenau, E. H., Pavelsky, T. M., Moller, D., Pitcher, L. H., Bates, P. D., Durand, M. T., & Smith, L. C. (2019). Temporal variations in river water surface elevation and slope captured by AirSWOT. *Remote Sensing of Environment*, *224*, 304–316. https://doi.org/10.1016/j.rse.2019.02.002.

Andreadis, K. M., Schumann, G. J. P., Stampoulis, D., Bates, P. D., Brakenridge, G. R., & Kettner, A. J. (2017). Can atmospheric reanalysis data sets be used to reproduce flooding over large scales? *Geophysical Research Letters*, *44*, 10,369–10,377. https://doi.org/10.1002/2017GL075502

Bates, P. D., Neal, J. C., Alsdorf, D., & Schumann, G. J.-P. (2014). Observing global surface water flood dynamics. *Surveys in Geophysics*, *35*(3), 839–852. https://doi.org/10.1007/s10712-013-9269-4

Biancamaria, S., Hossain, F., & Lettenmaier, D. P. (2011). Forecasting transboundary river water elevations from space. *Geophysical Research Letters*, *38*, L11401. https://doi.org/10.1029/2011GL047290

Biancamaria, S., Lettenmaier, D. P., & Pavelsky, T. M. (2016). The SWOT mission and its capabilities for land hydrology. *Surveys in Geophysics*, *37*(2), 307–337. https://doi.org/10.1007/s10712-015-9346-y

Bonnema, M., & Hossain, F. (2017). Inferring reservoir operating patterns across the Mekong basin using only space observations. *Water Resources Research*, *53*, 3791–3810. https://doi.org/10.1002/2016WR019978

Brakenridge, G. R. (2018). Flood risk mapping from orbital remote sensing. In G. J. P. Schumann, P. D. Bates, H. Apel, & G. T. Aronica (Eds.), *Global flood hazard: Applications in modeling, mapping, and forecasting* (pp. 43–54). Hoboken, NJ: American Geophysical Union and John Wiley & Sons, Inc. https://doi.org/10.1002/9781119217886.ch3

Brakenridge, G. R., & Kettner, A. J. (2017). DFO flood event 4510. Retrieved from http://floodobservatory.colorado.edu/Events/2017USA4510/2017USA4510.html, (Accessed 19 August 2019).

Brakenridge, G. R., Knox, J. C., Paylor, E. D., & Magilligan, F. J. (1994). Radar remote sensing aids study of the Great Flood of 1993. *Eos, Transactions AGU*, *75* (45), 521–527. https://doi.org/10.1029/EO075i045p00521

Brakenridge, G. R., Tracy, B. T., & Knox, J. C. (1998). Orbital SAR remote sensing of a river flood wave. *International Journal of Remote Sensing*, *19* (7), 1439–1445. https://doi.org/10.1080/014311698215559

Brisset, P., Monnier, J., Garambois, P.-A., & Roux, H. (2018). On the assimilation of altimetric data in 1d Saint–Venant river flow models. *Advances in Water Resources*, *119*, 41–59. https://doi.org/10.1016/j.advwatres.2018.06.004

Chen, B., Krajewski, W. F., Goska, R., & Young, N. (2017). Using lidar surveys to document floods: A case study of the 2008 Iowa flood. *Journal of Hydrology*, *553*, 338–349. https://doi.org/10.1016/j.jhydrol.2017.08.009

Desai, S. (2018). Surface Water and Ocean Topography mission (SWOT), science requirements document *Rep. JPL document D-61923 Revision B, https://swot.jpl.nasa.gov/docs/D-61923_SRD_Rev_B_20181113.pdf*, 29 pp, Jet Propulsion Laboratory.

Domeneghetti, A., Schumann, G. J. P., Frasson, R. P., Wei, R., Pavelsky, T. M., Castellarin, A., et al. (2018). Characterizing water surface elevation under different flow conditions for the upcoming SWOT mission. *Journal of Hydrology*, *561*, 848–861. https://doi.org/10.1016/j.jhydrol.2018.04.046

Domeneghetti, A., Tarpanelli, A., Brocca, L., Barbetta, S., Moramarco, T., Castellarin, A., & Brath, A. (2014). The use of remote sensing-derived water surface data for hydraulic model calibration. *Remote Sensing of Environment*, *149*, 130–141. https://doi.org/10.1016/j.rse.2014.04.007.

Durand, M., Fu, L. L., Lettenmaier, D. P., Alsdorf, D., Rodríguez, E., & Esteban-Fernandez, D. (2010). The Surface Water and Ocean Topography mission: Observing terrestrial surface water and oceanic submesoscale eddies. *Proceedings of the IEEE*, *98*(5), 766–779. https://doi.org/10.1109/jproc.2010.2043031

Esteban-Fernandez, D. (2013). SWOT mission performance and error budget *Rep. JPL D-79084 Revision A, https://swot.jpl.nasa.gov/files/SWOT_D-79084_v5h6_SDT.pdf*, Jet Propulsion Laboatory.

Fjørtoft, R., Gaudin, J.-M., Pourthie, N., Lalaurie, J.-C., Mallet, A., Nouvel, J.-F., et al. (2014). KaRIN on SWOT: Characteristics of near-nadir Ka-band interferometric SAR imagery. *IEEE Transactions on Geoscience and Remote Sensing*, *52*(4), 2172–2185. https://doi.org/10.1109/tgrs.2013.2258402

Frasson, R. P. d. M., Pavelsky, T. M., Fonstad, M. A., Durand, M. T., Allen, G. H., Schumann, G., et al. (2019). Global relationships between river width, slope, catchment area, meander wavelength, sinuosity, and discharge. *Geophysical Research Letters*, *46*(6), 3252–3262. https://doi.org/10.1029/2019GL082027

Frasson, R. P. d. M., Wei, R., Durand, M., Minear, J. T., Domeneghetti, A., Schumann, G., et al. (2017). Automated river reach definition strategies: Applications for the Surface Water and Ocean Topography mission. *Water Resources Research*, *53*, 8164–8186. https://doi.org/10.1002/2017wr020887

Gleason, C. J., & Hamdan, A. N. (2015). Crossing the (watershed) divide: Satellite data and the changing politics of international river basins. *The Geographical Journal*, *183*, 2–15. https://doi.org/10.1111/geoj.12155

Hossain, F., Siddique-E-Akbor, A. H., Mazumder, L. C., ShahNewaz, S. M., Biancamaria, S., Lee, H., & Shum, C. K. (2014). Proof of concept of an altimeter-based river forecasting system for transboundary flow inside Bangladesh. *Ieee Journal of Selected Topics in Applied Earth Observations and Remote Sensing*, *7*(2), 587–601. https://doi.org/10.1109/jstars.2013.2283402

Kollasch, P. (2009). Flood extent from spot satellite data of the Iowa and Cedar Rivers, including Iowa City and Cedar Rapids, in east-central Iowa on June 17, 2008. Iowa City, Iowa. ftp://ftp.igsb.uiowa.edu/gis_library/projects/flood_2008/flood_extent_iowa_cedar_20080617.zip

Kundzewicz, Z. W., Pinskwar, I., & Brakenridge, G. R. (2013). Large floods in Europe, 1985–2009. *Hydrological Sciences Journal*, *58*(1), 1–7. https://doi.org/10.1080/02626667.2012.745082

Mallakpour, I., & Villarini, G. (2015). The changing nature of flooding across the central United States. *Nature Climate Change*, *5*(3), 250–254. https://doi.org/10.1038/nclimate2516

Nardi, F., Annis, A., Di Baldassarre, G., Vivoni, E. R., & Grimaldi, S. (2019). Gfplain250m, a global high-resolution dataset of Earth's floodplains. *Scientific Data*, *6*(1), 180309. https://doi.org/10.1038/sdata.2018.309

Oubanas, H., Gejadze, I., Malaterre, P.-O., Durand, M., Wei, R., Frasson, R. P. d. M., & Domeneghetti, A. (2018). Discharge estimation in ungauged basins through variational data assimilation: The potential of the SWOT mission. *Water Resources Research*, *54*, 2405–2423. https://doi.org/10.1002/2017WR021735

Pavelsky, T. M., Durand, M., Andreadis, K. M., Beighley, R. E., Paiva, R. C. D., Allen, G. H., & Miller, Z. F. (2014). Assessing the potential global extent of SWOT river discharge observations. *Journal of Hydrology*, *519*, 1516–1525. https://doi.org/10.1016/j.jhydrol.2014.08.044

Pielke, R. A., & Downton, M. W. (2000). Precipitation and damaging floods: Trends in the United States, 1932–97. *Journal of Climate*, *13*(20), 3625–3637. https://doi.org/10.1175/1520-0442(2000)013<3625:padfti>2.0.co;2

Quinn, N., Bates, P. D., Neal, J., Smith, A., Wing, O., Sampson, C., et al. (2019). The spatial dependence of flood hazard and risk in the United States. *Water Resources Research*, *55*(3), 1890–1911. https://doi.org/10.1029/2018wr024205

Risser, M. D., & Wehner, M. F. (2017). Attributable human-induced changes in the likelihood and magnitude of the observed extreme precipitation during Hurricane Harvey. *Geophysical Research Letters*, *44*, 12,457–12,464. https://doi.org/10.1002/2017GL075888

Rodríguez, E. (2015). Surface Water and Ocean Topography mission (SWOT), science requirements document *Rep. JPL document D-61923, https://swot.jpl.nasa.gov/files/swot/SRD_021215.pdf*, Jet Propulsion Laboratory.

Shastry, A., & Durand, M. (2019). Utilizing flood inundation observations to obtain floodplain topography in data-scarce regions. *Frontiers in Earth Science*, *6*. https://doi.org/10.3389/feart.2018.00243

Smith, J. A., Baeck, M. L., Villarini, G., Wright, D. B., & Krajewski, W. (2013). Extreme flood response: The June 2008 flooding in IOWA. *Journal of Hydrometeorology*, *14*(6), 1810–1825. https://doi.org/10.1175/jhm-d-12-0191.1

Sneddon, C., & Fox, C. (2006). Rethinking transboundary waters: A critical hydropolitics of the Mekong basin. *Political Geography*, *25*(2), 181–202. https://doi.org/10.1016/j.polgeo.2005.11.002

Sneddon, C., & Fox, C. (2012). Water, geopolitics, and economic development in the conceptualization of a region. *Eurasian Geography and Economics*, *53*(1), 143–160. https://doi.org/10.2747/1539-7216.53.1.143

Tarpanelli, A., Camici, S., Nielsen, K., Brocca, L., Moramarco, T., & Benveniste, J. (2019). Potentials and limitations of Sentinel-3 for river discharge assessment. *Advances in Space Research*. https://doi.org/10.1016/j.asr.2019.08.005

Tuozzolo, S., Lind, G., Overstreet, B., Mangano, J., Fonstad, M., Hagemann, M., et al. (2019). Estimating river discharge with swath altimetry: A proof of concept using AirSWOT observations. *Geophysical Research Letters*, *46*, 1459–1466. https://doi.org/10.1029/2018GL080771

Van Dijk, A. I. J. M., Brakenridge, G. R., Kettner, A. J., Beck, H. E., De Groeve, T., & Schellekens, J. (2016). River gauging at global scale using optical and passive microwave remote sensing. *Water Resources Research*, *52*, 6404–6418. https://doi.org/10.1002/2015wr018545

Wing, O. E. J., Bates, P. D., Smith, A. M., Sampson, C. C., Johnson, K. A., Fargione, J., & Morefield, P. (2018). Estimates of present and future flood risk in the conterminous united states. *Environmental Research Letters*, *13*, 034023. https://doi.org/10.1088/1748-9326/aaac65

Wolf, A. T., Natharius, J. A., Danielson, J. J., Ward, B. S., & Pender, J. K. (1999). International river basins of the world. *International Journal of Water Resources Development*, *15*(4), 387–427. https://doi.org/10.1080/07900629948682

Zhang, W., Villarini, G., Vecchi, G. A., & Smith, J. A. (2018). Urbanization exacerbated the rainfall and flooding caused by Hurricane Harvey in Houston. *Nature*, *563*(7731), 384–388. https://doi.org/10.1038/s41586-018-0676-z